Hydro-thermal phenomena of oil-multi-walled carbon nanotubes nano-fluid flow through a rectangular channel: impact of obstacles

Shahul Hameed[1], Sandip Saha[1*]

[1]Division of Mathematics, School of Advanced Sciences, Vellore Institute of Technology Chennai, Tamilnadu-600127, India

*E-mail: sandip.saha@vit.ac.in

Abstract

Thermo-hydraulic analysis of nano-fluid flow phenomena through rectangular channels has currently created much interest among researchers, and is being used in a variety of engineering applications (including glass blowing, and continuous metal casting, especially in a variety of manufacturing processes like transpiration cooling, and laser pulse heating). The hydrothermal properties of nano-fluid flow in a rectangular channel embedded with obstacles under uniform heat flux have been studied numerically with the variations of the values of Reynolds numbers (Re) and different forms of obstacle. The governing equations have been solved using the finite volume approach, and fluent software has been used to visualize the simulation results. The impact of various forms of obstacle (plane, trapezoidal, elliptical, and triangular), the volume fraction of nano-particle (D%), and Re on the different thermo-hydraulic fluid flow phenomena have been investigated numerically. At $Re = 1, 60, 120$, and $D\% \in [0-4]$, the distributions of flow velocity, absolute pressure drop (Δp), temperature profile, average friction factor (f), local Nusselt number $\left(Nu(x)\right)$, and average Nusselt number $\left(Nu_{avg}\right)$ have been demonstrated for all the forms of obstacle. It has been discovered that, in terms of the various characteristics of hydrothermal flow phenomena, plane obstacles are more pronounced, whereas elliptical obstacles are less pronounced.

Keywords: Heat transfer; Nano-fluid flow; Volume fraction; Simulation; Obstacles.

1. Introduction

At present, rising energy consumption and fossil fuels have become essential in terms of living and well-being. Such consumption also has an effect on greenhouse gas production, air pollutant emissions, and natural resource depletion in many countries [1]. Efficient processes and industrial methods of HT [2] have now minimized environmental degradation and the advancement of technology in different industries has made it important for heat exchangers to decrease the size and eventually increase energy and fuel efficiency [3-5]. Compact heating system development has emerged in recent years as a critical and difficult goal for increasing efficiency across a range of industries [5-7]. The use of nano-fluids instead of water is one of the best ways to solve this problem. Innovative and impressive methods for the improvement of HT include the use of metallic and non-metallic particles in the base fluid, known as nano-fluid. In the works [8-11], authors have discussed HE and HT in electronic devices because of its importance in today's world. Many policies have been designed so far to increase the rate of thermal exchange, like the use of extended surfaces, rough surfaces, corrugated channels, and different forms of obstacles and grooves [12-14]. There is a necessity to increase HT capacities in existing systems and nano-fluids made of metallic and non-metallic particles in a base fluid are being used to do it. Furthermore, the utilization of nano-fluids has started in a new era in the industry [14-17]. Using nano-fluids, various authors [18-20] have improved the thermal efficiency of flow through channels. Inclusion of obstacles to the surfaces of HT systems is a common way to save costs; however, this always increases the size and volume of the system. Nano-fluids, in comparison to current HT technologies, provide a greater HT with low cost or without any drop in absolute pressure [21-23].

In the year 2021, Promvonge et al. [13] observed the influence of arc-shaped obstacle on the thermo-hydraulic performance of duct mounted with arc-shaped obstacle turbulators at different attached angles $(20^0, 40^0, 60^0\ and\ 90^0)$. At $Re = 4{,}000$, they noted that for 90^0 attachment angle, the thermal performance factor becomes highest, viz. 1.4. In 2022, Eiamsa-ard [14] numerically studied the HT mechanism and flow topology of channels with V-shaped obstacles and semi-circular hinged V-shaped obstacles for different pitch ratios (PR), blockage ratios, and semi-circular hinge angle (α). They stated that a thermal boundary layer was disrupted; and fluid mixing was promoted as a result of the VB’s solely primary vortex flow, which also improved HT. An increase in Re and BR causes the pressure drop and increase in HT. In addition, they revealed that at $\alpha = 10^0$, the values of Nu/Nu_0 and TEF become maximum. Some excellent results by renowned Professors are demonstrated in table 1, which are more effective in developing the current field / new era of research.

After going through the above discussions, it is obvious that nano-fluid plays an important role in the cooling industry for studying the different hydrothermal flow characteristics. Notwithstanding the considerable potential of nano-fluid flow through rectangular channel with obstacles, enough research has not been done. The literature review reveals that most of the works have been completed without considering the influence of the various obstacle configurations, Re, D%, and effect of baffle-obstacle corrugation on the distributions of flow velocity, Δp, temperature profile, $f, Nu(x)$, and Nu_{avg}. It seems that the unexplored areas of research are still there as the above-mentioned investigations are considered nano-fluid flow in a rectangular channel in presence of single obstacle configuration, and analyzed different characteristics of flow phenomena only, which provides us enough confidence to implement the current idea. With this in mind, here we have numerically studied the various thermo-hydraulic phenomena of oil-MWCNT nano-fluid flow through a rectangular channel embedded with obstacle of various shapes, and multiple number of obstacle configurations. The following points have not been covered in the previously released publications.

i) To study the influence of Re on various characteristics of thermo-hydraulic fluid flow phenomena (flow velocity, Δp, temperature profile, $f, Nu(x)$, and Nu_{avg}).

ii) To investigate the influence of $D\%$ on various characteristics of thermo-hydraulic fluid flow phenomena (flow velocity, Δp, temperature profile, $f, Nu(x)$, and Nu_{avg}).

iii) To study the influence of various forms obstacle configuration (plane, trapezoidal, elliptical, and triangular) on various characteristics of thermo-hydraulic fluid flow phenomena (flow velocity, Δp, temperature profile, $f, Nu(x)$, and Nu_{avg}).

iv) A comparative study has been performed to determine which obstacle configuration provides a greater rate of HT by analyzing the Nu_{avg} profile.

v) A comparative investigation has been demonstrated to reveal the % increase of HT rate in the case of different forms of obstacle rectangular channel vs. smooth channel.

The aforementioned reasons encourage us to carry on the current work. The findings of this article are particularly beneficial to many technical communities, including the works in electronics, power stations, the development of aerospace and vehicles, turbo-machinery, and the cooling and heating of homes. Moreover, the findings of this study will be extremely beneficial in a variety of engineering applications, including glass blowing, fiber spinning, and continuous metal casting, especially in a variety of manufacturing processes like transpiration cooling, fabric cleaning, and laser pulse heating. This kind of flow, which is the subject of the current study, has applications in PV (photovoltaic) cells and collectors. The rectangular channel of the cooler, which is found at the bottom of PV collectors, is assumed to have one isolated side from which HT's through the other side that meets the PV collector. Overall, the D% of nano-fluid affects the efficiency of Photo Voltaic collectors, which can be seen in the result section that how D%, obstacle shape and Re influence the hydro-thermal phenomena in the rectangular cross-section. The conventional fluid and nano-fluid increase the efficiency of photovoltaic cells. The authors claim that no previous integrated effort of this nature has been done.

2. Problem statement

The geometry of the proposed problem is shown in figure 1. Here, a two-dimensional domain [29] has been used for the numerical simulations with a height $H = 0.05\ mm$ and a length $L = 0.0075\ m$. Figures

1(a-d) present the rectangular micro-channel embedded with four various obstacle configurations, which are referred as plane obstacles (figure 1a), trapezoidal obstacles (figure 1b), triangular obstacles (figure 1c), and elliptic obstacles (figures 1d). The channel consists of four sections, viz., inlet section, through which the flow enters into the system, lower wall, and upper wall and outlet section. A vortex generator in the form of an obstacle has been affixed to the channel wall at a distance of 0.385 cm from the channel's upstream end. The goal of this work is to model the flow of nano-fluids and HT in two-dimensional micro-channels with various forms of obstacles. The bottom wall of the micro-channel is insulated, but $q = 25{,}000\, W/m^2$ has been applied in the middle of the top wall (noted by red colour in figure 1), where the obstacles are placed. The insulated lengths of the top wall's inlet and exit are 0.375 cm and 0.225 mm, respectively. The obstacles pitch, height, and length are measured at 0.03, 0.002, and 0.01cm, respectively. $T_c = 298\, K$ is the working fluid's intake temperature. Additionally, it is proposed that the silver nano-particles and water are in a state of thermal equilibrium, and the nano-particles are spherical. Under a no-slip boundary condition in the walls, the flow along the micro-channel is laminar, Newtonian, and incompressible, and the influence of radiation is insignificant. Table 2 shows the thermo-physical characteristics of nanoparticles [24], nano-fluid, and distilled water (base fluid) at various volume fractions at an average temperature of 298 K. In this work, fluid flow and HT parameters have been calculated, and numerical calculations are performed for $Re = 1,\ 60, and\ 120$, with $D\% = 0, 2, 4.$ The height (H_1) and length (l_1) of obstacles have been taken into consideration as constants to provide a better comparison for each obstacle shape considered in this research. Figure 1(e) presents the rectangular geometry with generating plane $(l_5,$ and $l_6)$ for each of the obstacle shapes.

3. Mathematical modeling

As per the studies of [24, 29, 30], the dimensional equations, such as continuity (eq. 1), momentum of x (eq. 2), momentum of y (eq. 3), and temperature (eq. 4) have been taken to regulate the laminar steady state flow in a Cartesian coordinate system, which are as follows.

$$\frac{\partial u_1}{\partial x} + \frac{\partial v_1}{\partial y} = 0 \tag{1}$$

$$u_1 \frac{\partial u_1}{\partial x} + v_1 \frac{\partial u_1}{\partial y} = -\frac{1}{\rho_{nf_1}} \frac{\partial p_1}{\partial x} + \frac{\mu_{nf_1}}{\rho_{nf_1}} \left(\frac{\partial}{\partial x}(\frac{\partial u_1}{\partial x}) + \frac{\partial}{\partial y}(\frac{\partial u_1}{\partial y}) \right) \tag{2}$$

$$u_1 \frac{\partial v_1}{\partial x} + v_1 \frac{\partial v_1}{\partial y} = -\frac{1}{\rho_{nf_1}} \frac{\partial p_1}{\partial y} + \frac{\mu_{nf_1}}{\rho_{nf_1}} \left(\frac{\partial}{\partial x}(\frac{\partial v_1}{\partial x}) + \frac{\partial}{\partial y}(\frac{\partial v_1}{\partial y}) \right) \tag{3}$$

$$u_1 \frac{\partial T_1}{\partial x} + v_1 \frac{\partial T_1}{\partial y} = \alpha_{nf_1} \left(\frac{\partial}{\partial x} (\frac{\partial T_1}{\partial x}) + \frac{\partial}{\partial y} (\frac{\partial T_1}{\partial y}) \right) \quad (4)$$

Following the work of [28-30], thermo physical characteristics of nano-fluid has been calculated, as follows.

$$\rho_{nf_1} = (1-D)\rho_{f_1} + D\rho_{np_1} \quad (5)$$

$$(\rho c_p)_{nf_1} = (1-D)(\rho c_p)_{f_1} + D(\rho c_p)_{np_1} \quad (6)$$

$$\mu_{nf_1} = \mu_{f_1} / (1-D)^{2.5} \quad (7)$$

The effective thermal conductivity (k_{eff1}) of suspensions is computed as per the research of [31, 32].

$$k_{eff_1} = k_{f_1} \left[1 + \frac{D}{1-D} \frac{k_{np_1}}{k_{f_1}} \frac{d_{f_1}}{d_{np_1}} - 36000 \frac{k_{np_1}}{k_{f_1}} \frac{2Tk_b}{\pi d_{np_1} \mu_{f1} \alpha_{f_1}} \frac{D}{1-D} \frac{d_{f_1}}{d_{np_1}} \right] \quad (8)$$

3.1. Conditions at the boundary

The thermo-hydraulic boundary conditions have been chosen from the works of [29-32]. The considered domain is divided into three subsections, such as inlet, outlet, and wall sections.

- Inlet section: At the entry section: At the inlet of the computational domain, a uniform one-dimensional velocity ($u = u_0$), with initial temperature ($T_0 = 298K$) has been used as the hydraulic boundary condition.
- Outlet section: The pressure at the channel outlet has been assumed as zero gauge pressure, $\frac{\partial u_1}{\partial x} = 0$.
- At the walls: The channel walls ($y = 0$; $y = 0.000005m$) are subjected to no-slip and no-penetration boundary conditions. Arbitrarily, some part of the top wall (red colored part) of the rectangular domain has been kept at $q = 25{,}000\ W/m^2$ and the bottom wall is considered as insulated.

3.2. Numerical descriptions, grid study, and validation

The governing equations have been solved using the FVM taking into account all the variables, which are defined at the center of the control volume and populate the physical domain. A discrete equation connecting the variable at the center to its neighbors is produced by integrating each equation across each control volume. The finite volume technique has several enticing characteristics; however, there are several undesired numerical effects due to the low-order interpolation of the convective elements in the governing equations. The momentum equation's convective terms have been spatially discretized using the QUICK technique [33] to counteract those effects. It is an upwind scheme, with accuracy for advection terms being 3rd order, and accuracy for all other terms being 2nd order. The mass and momentum balances do not directly supply the equation that defines the pressure update, which is required for the solution procedure. As the SIMPLEC algorithm seeks to mitigate the effects of velocity neighbor correction terms, it resolves the coupling between the velocity and pressure. To ensure precise iteration numbers and control numerical in accuracy, a residual of 10^{-6} has been taken. The radiation impacts are minimal and the nano-fluid is homogenous in this simulation. To simulate the fluid flow and temperature fields; FLUENT, commercial CFD software has been utilized. The working procedure of SIMPLEC algorithm has been described in figure 2. Under-relaxation factor has been adjusted between 0.3 and 1.0 to manage the computation of the variables at each iteration. Until it attains the predetermined residuals or stabilizes at a fixed value, the solver again runs through the equations.

Using several constructed grids with varying numbers of nodes, simulations in the computational domain with plane obstacles have been done to examine grid independence. The mesh has been generated using fluent software. The mesh geometry of the rectangular channel embedded with six plane obstacles is shown in figure 3(a). This indicates that the mesh is too fine at the solid border, which is necessary to get the strong gradients in pressure and velocity. The independence of flow and HT characteristics is the purpose of this study. To capture the fluctuations in the flow and temperature fields within the hydraulic and thermal boundary layers, the grid density has been kept higher in the region of the heated wall and the obstacles. Grid test has been performed at $Re = 120$ for the case of the rectangular channel with plane obstacle. The goal of the grid independence test [figures 3(b, c)] is to identify the ideal grid for which the computational cost is minimal without affecting the correctness of the outcome. Here the chosen grid number has been examined between 8,484 and 25,000.The centerline average velocity (C_v), and average friction coefficient (f_{av}) on the indented wall with plane obstacles has been compared for various grid numbers for a selected grid number. Figures 3(b) and 3(c) show that the trend of C_v (figure 3b), and f_{av}(figure 3c) becomes linear and constant after $19{,}003\ N_e$, suggesting that $19{,}003\ N_e$ is sufficient to perform further investigation. It has been found that the grid number of 19,003 produces more accurate results than smaller grid numbers when the parameters in the chosen grid number are changed. For all the considered forms of obstacle, the same mesh system has been utilized. The current study has been validated by the numerical and experimental works done earlier to assess the correctness of the numerical solution technique and to regulate the degree of error in selecting the numerical scheme.

To check the accuracy of the results, the numerical simulations have been verified against the references [29 (Behnampour et al., numerical work), and 34 (Ahmed et al., experimental work),] considering the same geometric and boundary conditions of the current problem. Using the SIMPLEC algorithm and the FVM, Behnampour et al. [29] quantitatively studied the laminar flow of a water/Ag nano-fluid in a rectangular micro-channel with $D\% = [0 - 4]$. In [34], Ahmed et al. experimentally studied the profile of Nu_{avg} with the variations in Re for the case of double-layered obstacle in a rectangular channel. Validation [figure 4a,4b] of the current study has been done with the study of Behnampour et al. [29], and Ahmed et al. [34] by analyzing the profiles of Nu_{avg} vs. Re. From the figures 4(a, b), it has been investigated that Nu_{avg} in this investigation is quite consistent with the research conducted in references 29, and 34. In addition, it has been observed that the value of the Nu_{avg} increases with the increase in the values of Re. Moreover, due to the presence of solid nano-particles in between fluid layers, it is seen that the value of Nu_{avg} rises with the increase of the value of $D\%$. From figures 4(a, b), it can be concluded that the presence of nano-particles enhances the fluid's heat conductivity characteristics, and strengthens micron-scale HT mechanisms. Figures 4(a, b) show the strong agreement between the result of the current work and the results of [29, 34], which provides us the enough confidence to carry forward the present work.

4. Results and discussions

The impact of various geometric parameters especially the number of obstacles, and their shapes on the different characteristics of the thermo-hydraulic phenomena have been investigated. The effects of using various operating circumstances, such as Re, the shape of the obstacles, and D% on oil-MWCNT nano-fluids flow have been investigated.

4.1. Influence of obstacle shape, D%, and Re on hydro-thermal flow behavior

In this subsection, we have discussed the impacts of obstacle shapes (plane, trapezoidal, triangle, and elliptical), $D\%$, and Re on different characteristics of thermo-hydraulic fluid flow phenomena (profiles of velocity, pressure, temperature, $Nu(x), C_f(x),$ and Nu_{avg}) through a rectangular channel embedded with obstacle, and the findings have been computed for volume fractions of $D\% = [0 - 4]$, and $Re = 1, 60$ and 120. The impacts of obstacles on the generated gradient and flow characteristics have been demonstrated in figure 5. For different shapes of the obstacles, the velocity distribution contours have been presented at $Re = 120$, and $D\% = 4.00$, as shown in figures 5(a, c, and e). The flow reaches a hydrodynamic fully developed regime once it enters the channel. The gradients, which are formed behind the installed obstacles, lead to improved mixture flow, which in turn enhances heat transmission. It has been observed that velocity contours alter in certain ways for using obstacles with sharp-angle surfaces. The interaction of the fluid with the obstacles forms several eddies and notable changes in the axial velocity gradient. When the fluid encounters the obstacles; it is redirected, leading to an increase in the vertical component of the velocity. Interaction of the fluid with the tip of the obstacles increases the velocity gradient, which causes abrupt shifts in velocity. Variation in the velocity increases as the fluid reaches the subsequent obstacle corner. In general, obstacle types with more corners alter velocity gradients more quickly than triangular ones do. Furthermore, there are also strong whirlpools that occur in the rear of the obstacles, and the most dramatic one occurs in the rear of the trapezoidal and rectangular obstacles. From the figures 5(a, c, e), it has been found that the velocity value becomes maximum in the case of the plane obstacle rectangular channel as compared to the other considered cases. Figures 5(b, d, f) show the temperature contours at $Re = 120$, and $D\% = 4.00$. According to the figures 5(b, d, f), HT occurs between the fluid and obstacle-roughened surfaces when a fluid with a temperature T_0 reaches obstacle-roughened portions with a cold surface. This reduces the fluid temperature. As the Re, the rate of HT increases. This is because the heated fluid remains in contact with a cold surface for long at low Re. HT increases as the fluid crosses the obstacle tip because of improved flow mixing. An increase in D% and the presence of obstacles result in an overall increase in HT rate. Due to increased thermal conductivity at increasing D%, the temperature rises for all modes under study in a region close to the entrance.

The cause of these phenomena is the corresponding increase in micronic heat transmission mechanisms with the intensification of the nano-fluid D%. Positive effects on the mixing of nano-fluid are also attributed to various obstacle shapes throughout the flow. In addition, it has been demonstrated that in the case of plane obstacles, temperature becomes higher as compared to the other considered cases. Therefore, from figure 5, it has been concluded that for obtaining improved flow mixing in such type of obstacle channels, plane obstacles become more effective. At $Re = 60$ and 120, the profiles of axial velocity along the centerline of the channel have been shown in figures 6, 7 for different configurations of the obstacles. The simulation results show that around the obstacle-roughened areas, dimensional velocity increases as the obstacles block the cooling fluid's flow in the channel. Velocity fluctuations have been noticed to be higher at $Re = 120$ as compared to the case of $Re = 60$, as seen in figures 6, 7 as higher value Re improves flow integration with the obstacle-roughened surface. It has been noticed that the axial velocity profiles vary with the shape of the obstacles. It has also been noticed that the variations in the profile of axial velocity are found more pronounced in presence of plane obstacles. The interaction between fluid and obstacles generates axial velocity gradient, and forms eddies. It has been noticed that the fluid velocity reaches to its maximum at the obstacle tips. It is obvious from the figure 5 that the variations in velocity profile become higher when the fluid touches the next obstacle.

After passing the first obstacle, the flow approaches towards the base of the second obstacle at a faster speed, and the flow field is deformed eminently. As a result, the flow is quite high at the tip of the second obstacle and gets even higher at the tip in the proximity of the third obstacle. For all the forms of the obstacle, it is found that the flow velocity profile becomes more reinforced at $l_6 = 0.00565\ m$ rather than $l_5 = 0.00415\ m$. Moreover, at $Re\ =\ 120$ and $D\%\ =\ 0$, it has been found that maximum flow velocity attains nearly 1.4794 times of the inflow velocity for the presence of plane obstacle at $l_5 = 0.00415\ m$, while the maximum flow velocity becomes 1.4816 times of the inflow velocity for the same case at $l_6 = 0.00565\ m$ as can be seen from the table-3, and table-4. At $Re\ =\ 60$, 120 and for different values of $D\%$, the figures 8 and 9 demonstrate the variations of static pressure profiles along the centerline for different types of obstacle. The intensity of the fluid mixture increases, when the fluid passes over the obstacles. In addition, fluid velocity diminishes due to the interaction of the fluid with the surface, which causes an increase in the values of static pressure. Moreover, the presence of obstacles affects the hydrodynamic flow behavior of cooling fluid.

The obstacles in the channel create velocity gradient near the wall, which diffuses and transmits momentum to alter the flow within the channel. As the fluid flows from the upstream to downstream, its normal flow is disrupted due to the presence of obstacles. As a result, the volume of fluid mixture is improved. On the other hand, fluid momentum reduces because of the fluid's interaction with the surface, and due to that, the pressure drop increases. The momentum drop rises with the increase in the fluid velocity. Additionally, the hydrodynamic behavior of fluid flow is influenced by the presence of different shaped obstacles. As Re decreases from 120 to 60, there is a decrease in the impressionability of pressure variations brought on by obstacle form. The primary cause of this is that the fluid is moving more slowly and experiences less variation in velocity when it interacts with the barriers. With the variations of D%, and obstacle configuration, the figures 10 and 11 present the plots of temperature profile along the centerline at $Re = 1$, and $Re =\ 60$. Variations in the temperature profile have been noticed along the centerline of the flow when obstacles are on the heated surfaces and the flow strikes the obstacles. At $Re = 10$, the fluid flows slowly and takes a long time to transfer heat from hot surfaces to cooling fluid, and in this case graphs of temperature are found related to the forms of the obstacles someway. An increase in the fluid velocity reduces temperature significantly, and due to this growth of the thermal boundary layer decreases. This results in reduction in hot surfaces along the centre line of the flow. An increase in the $D\%$ and Re dominates inlet fluid's temperature inside the micro channel. The profiles of temperature barely change at all. Nevertheless, a rise in the flow velocity causes the temperature gradients to drastically alter and move towards the center of the flow field. The highest change in temperature gradient has been found in the case of the plane obstacle. The presence of obstacles results in an improvement in the integration of fluid layers, decreased temperature along the channel, and a consequent rise in heat transmission. Moreover, an increase in Re, and the existence of obstacles causes an enhancement in temperature gradient significantly, which changes the direction of the flow field towards the centerline. An increase in Re causes a significant decrease in the temperature, which in turn reduces the thickness of the thermal boundary layer of the hot surfaces of the centerline flow. It is also found that an increase in D% causes an increase in the temperature as the thermal conductivity increases. Variations of Δp_1 at different values of Re, and for different types of obstacles have been presented in the figures 12(a-d). The graph demonstrates how obstacle formation significantly affects pressure loss. At all Re under investigation, there is a substantial rise in pressure loss with increasing fluid viscosity and D%. It has been found that the plane obstacles result in the greatest pressure loss. In addition, due to a quick change in pressure over the top of the obstacle, the elliptical obstacle experiences the lowest value of Δp_1. However, for other obstacle shapes, the pressure changes over a longer region because of the upper side of the obstacle.

The findings show that an increase in pressure loss is closely correlated with Re and D%, which is caused by the working fluid's increased viscosity and density. Pressure gradient increases due to the fluid-obstacle interaction, which causes the fluid velocity to decrease and the pressure drop to rise. The presence of obstacles in the direction of fluid flow induces the damping of momentum and the loss of kinetic energy of the fluid. In addition, the presence of an obstacle increases velocity gradients and absolute pressure drop in the direction of fluid motion. The plots of f for various obstacle shapes have been shown in the figures 12(e-f). It has been demonstrated that the value of f rises as the D% and Re increases. This results in an increase in the density that follows a larger D%. When compared to base fluid, nano-fluids exhibit greater velocity loss as the flow encounters obstacles, which is the primary cause of the higher f at a higher D%. Moreover, the highest f growth has been found in the case of rectangular and trapezoidal obstacles due to the differences in velocity at the obstacle corners. A decrease in the Re causes the cooling fluid to come into touch with the surface more slowly, which increases the impact of shear stress between the fluid and the obstacle-roughened surface in the fluid layer close to the surface. The f values at different D% and for different forms of obstacle have been figured out in table 5. It is observed that % increase in$f$, due to an increase in D% for triangular obstacle become more prominent than the case of others. At $Re = 60, 120$ and D%=0, figures 13(a, b) presents the variation in $C_f(x)$ for all considered cases to show the impact of obstacles in the profile of $C_f(x)$. In all the instances, the $C_f(x)$ decreases as Re rises. This hydrodynamic behavior is caused by the difference in velocity values at lower Re. The fluid has greater time to meet the obstacle surfaces at lower Re. Furthermore, any variation in the fluid's velocity is more noticeable. Higher Re causes a small variance in velocity factors because the flow momentarily makes contact with obstacle surfaces along the passage, allowing the flow in contact with a portion of the obstacle. Plane and trapezoidal obstacles have the biggest variety of $C_f(x)$ and the greatest velocity fluctuations. It has been noted that the creation of large vortices in the region close to the baffle tips causes the coefficient of friction to drop off quickly. It is evident that the $C_f(x)$ curves rise in the areas of counter-rotating flow zones. Due to the existence of a tiny recycling cell, the friction values are raised in the region close to the left side of the obstacles, and subsequently continue to decrease at the obstacles base. Furthermore, the presence of six obstacles causes the occurrence of six peaks, as seen in the figure 13(a, b). For all considered obstacle cases, figure 14 reflects the plots of $Nu(x)$ at several values of Re, and $D\% = 0$. It has been found that the profiles of $Nu(x)$ become more pronounced with the increase in the values of Re. The fluid's deviation from its intended direction during its interaction with the obstacles caused notable alterations in the velocity parameters, which in turn affected the HT coefficient and $Nu(x)$. It is evident from all the $Nu(x)$ graphs that the principal obstacles exhibit the highest rate of abrupt fluctuations in $Nu(x)$, which are subsequently mitigated by the decrease in fluid momentum caused by the fluid's interaction with other obstacles.

Additionally, the $Nu(x)$ graphs are significantly altered by the shape of obstacles; hence, the presence of obstacles with acute angles results in abrupt changes in these figures. It has been noticed that at $Re = 1$, fluid does not experience the effects of obstacles due to the low velocity of the fluid. The occurrence of more thermally conductive nano-particles and the impact of Brownian motion on the thermal conductivity of nano-fluid cause this rise. Another component that raises the Nu(x) and causes a sharp rise in obstacle-roughened areas is the presence of obstacles. The improved mixing of fluid layers between hot and cool regions is the primary cause of this increase. The thermal barrier layer is disrupted and altered when the fluid passes over the obstacles which eventually increase the rate of heat transmission. It has also been found that the maximum changes in the Nu(x) occur in the case of plane obstacles. Figure 15 demonstrates the plots of Nu_{avg} in all the considered cases at several values of Re. It has been confirmed that the increase in the values of D% and Re causes an increase in the values of Nu_{avg}. For each of the cases under study, the Nu_{avg} rises significantly at $Re = 120$ due to the enhancement of fluid layer mixing and HT. It is found that for a change in the values of $D\%$, the base fluid induces a change in the coefficient of CHT and causes an increase in the value of Nu_{avg}. The shape of the obstacles induces major differences in HT enhancement at $Re = 60$ and 120, but those are not significant at $Re = 1$. Moreover, the % increase in Nu_{avg} has been shown in table-6 to investigate the impacts of different obstacle shapes on the profile of Nu_{avg}. At $Re = 120$, it has been observed that maximum values of Nu_{avg} occur in presence of the plane obstacles, and the minimum value of Nu_{avg} attains in the presence of elliptical obstacles as velocity gradients exist along the flow direction (table-6).

Conclusion

In the current work, the thermo-hydraulic phenomena of oil-FMWCNT nano-fluid flow through a rectangular channel with obstacles have been studied numerically with the variations of D%, Re, and different shapes of obstacles. The concluding remarks are as follows:

- Based on the research conducted, it has been concluded that a raise in the values of Re, D%, and the presence of obstacles increase the heat transmission rate. At $Re = 120$ and $D\% = 0$, it has been investigated that maximum flow velocity becomes approximately 1.4794 times the input velocity in the case of plane obstacle at $l_5 = 0.00415\ m$. It has concluded that the variations in the profile of axial velocity and temperature are found more pronounced in the case of plane obstacles.
- The deviation in the direction of the fluid flow caused by the collision with the obstacles significantly altered the velocity parameters, which in turn affected the HT coefficient and Nusselt number.
- It has been found that the axial velocity contours vary significantly due to the presence of obstacles. Compared to other considered obstacles, higher axial velocity gradients are observed in the case of plane obstacles. In addition, it has been concluded that the obstacle shapes have a big impact on pressure loss.
- It has been revealed that an increase in Re causes a significant decrease in the temperature, which in turn reduces the thickness of the thermal boundary layer of the hot surface of the center line flow.
- For all values of Re, a substantial rise in pressure drop has been found with the increase in the fluid viscosity and $D\%$. Moreover, it has been demonstrated that the value of f rises as the $D\%$ and Re increases.
- It has been demonstrated that the $C_f(x)$ decreases as the Re rises. It has been noted that the creation of large vortices close to the obstacle tips causes the coefficient of friction to drop off quickly. Furthermore, six peaks have been found due to the presence of six obstacles.
- In the case of plane obstacles and $Re = 120$, it has been found that the value of Nu_{avg} at $D\% = 4$become 2.867 times of that at$D\% = 0$. Furthermore, in the case of the improved HT and the value of Nu_{avg}, the performance of obstacles is found as follows:

plane obstacle > trapezoidal obstacle > triangular obstacle > elliptical obstacle.

The current study's findings will be extremely beneficial in a variety of engineering applications, including glass blowing, fiber spinning, and continuous metal casting, especially in a variety of manufacturing processes like transpiration cooling, fabric cleaning, and laser pulse heating.

Conflict of interest

None

Funding

None

Acknowledgement

We really appreciate insightful comments of all the reviewers, which helped a lot to elevate the caliber of the work.

Reference

1. Khan, H.Z., Khan, A.W., Haq U.R., et al. “Effects of volume fraction on water-based carbon nanotubes flow in a right-angle trapezoidal cavity: FEM based analysis”, Int. Commun. Heat Mass Tran, **116**, pp. 104640, (2020).

2. Kimura S., Bejan, A.“The “Heatline” Visualization of Convective Heat Transfer”, J. Heat Transfer, **105(4)**, pp. 916-919, (1983).

3. Esfe, H.M., Rostamian, H., Toghraie, D., et al.“Numerical study of heat transfer of U-shaped enclosure containing nanofluids in a porous medium using two-phase mixture method”, Case Studies in Thermal Engineering, **38**, pp. 102150, (2022).

4. El-Shorbagy, A.M., Eslami, F., Ibrahim, M., et al. “Numerical investigation of mixed convection of nanofluid flow in a trapezoidal channel with different aspect ratios in the presence of porous medium”, Case Stud. Therm. Eng, **25**, pp. 100977, (2021).

5. Van Doormaal,P.J., Raithby, G.D. “Enhancements of the SIMPLEC method for predicting incompressible fluid flows”, Numerical Heat Transfer, **7**, pp. 147-163, (1983).

6. Bedram, A.“A novel method (a tube with successive increase and reduction in diameter) to increase nanofluid heat transfer in a tube”, Scintia Iranica, Articles in Press, **30,** (2023).

7. Khan, A.Z.M., Aziz, M., Wijayanta, T.A.“Prediction of heat transfer enhancement of delta-wing tape inserts using artificial neural network”, Case Studies in Thermal Engineering, **27**, pp. 101322, (2021).

8. Irene, K., Kristiawan, B., Enoki, K., et al.“Impact of nanoparticles loading to a novel hybrid TiO_2-CNTs/water nanofluid on thermal performance enhancement”, Numerical Heat Transfer, Part A: Applications, pp. 1-19, (2023).

9. Sutanto, B., Kristiawan, B., Yaningsih, I., et al.“Numerical approach of TiO_2 and CNT nanofluids flowing in circular, rectangular, and triangular tubes”, AIP Conference Proceedings, **2674 (1)**, (2023).

10. Boroomandpour, A., Toghraie, D., Hashemian, D.“A comprehensive experimental investigation of thermal conductivity of a ternary hybrid nanofluid containing MWCNTs- titania-zinc oxide/water-ethylene glycol (80:20) as well as binary and mono nanofluids”, Synthetic Metals, **268**, pp. 116501, (2020).

11. Yan, R.S., Toghraie, D., Abdulkareem, A.L., et al. “The rheological behavior of MWCNTs-ZnO/Water–Ethylene glycol hybrid non-Newtonian nanofluid by using of an experimental investigation”, Journal of Materials Research and Technology, **9(4)**, pp. 8401-8406, (2020).

12. Tian, S., Arshad, I.N., Toghraie, D., et al.“Using perceptron feed-forward Artificial Neural Network (ANN) for predicting the thermal conductivity of graphene oxide-Al_2O_3/water-ethylene glycol hybrid nanofluid”, Case Studies in Thermal Engineering, **26**, pp. 101055, (2021).

13. Promvonge, P., Eiamsa-ard, S., Wongcharee, K., et al. “Characterization of heat transfer and artificial neural networks prediction on overall performance index of a channel installed with arc-shaped baffle turbulators”, Case Stud Therm Eng, **26**, pp. 101067, (2021).

14. Eiamsamard, S., Suksangpanomrung, A., Promthaisong, P., “Enhanced heat transfer mechanism and flow topology of a channel contained with semi-circular hinged V-shaped baffles”, Int J Therm Sci, **177**, pp. 107577, (2022).

15. Wijayanta, T.A., Yaningsih, I., Juwana, E.W., et al. “Effect of wing-pitch ratio of double-sided delta-wing tape insert on the improvement of convective heat transfer”, International Journal of Thermal Sciences, **151**, pp. 106261, (2020).

16. Wijayanta, T.A., Yaningsih, I., Juwana, E.W., et al. “Double-sided delta-wing tape inserts to enhance convective heat transfer and fluid flow characteristics of a double-pipe heat exchanger”, Applied Thermal Engineering,**145**, pp. 27-37, (2018).

17. Yaningsih, I., Wijayanta, T.A., Miyazaki, T., et al. "Thermal hydraulic characteristics of turbulent single-phase flow in an enhanced tube using louvered strip insert with various slant angles”, International Journal of Thermal Sciences, **134**, pp. 355-362, (2018).

18. Kristiawan, B., Enoki, K., Juwana, E.W., et al. “Simulation-based assessment of the thermal-hydraulic performance of titania-based nanofluids in a circular-mini-channel tube”, International Journal of Ambient Energy, **43 (1),** pp. 8022-8035, (2022).

19. Kristiawan, B., Wijayanta, T.A., Enoki, K., et al. “Heat Transfer Enhancement of TiO2/Water Nanofluids Flowing Inside a Square Minichannel with a Microfin Structure: A Numerical Investigation”, Energies, **12(16)**, pp. 3041, (2019).

20. Kristiawan, B., Santoso, B., Aziz, M., et al.“Heat Transfer Enhancement of TiO_2/Water Nanofluid at Laminar and Turbulent Flows: A Numerical Approach for Evaluating the Effect of Nanoparticle Loadings”, Energies, **11 (6)**, pp. 1584, (2018).

21. Kristiawan, B., Rifa'I, I.A., Enoki, K., et al.“Enhancing the thermal performance of TiO2/water nanofluids flowing in a helical microfin tube”, Powder Technology, **376**, pp. 254-262, (2020).

22. Kurnia, C.J, Chaedir, B., Wijayanta, T.A., et al."Convective Heat Transfer Enhancement of Laminar Herschel–Bulkley Non-Newtonian Fluid in Straight and Helic Heat Exchangers with Twisted Tape Inserts", Ind. Eng. Chem. Res, **61(1)**, pp. 814–844, (2022).

23. Khodabandeh, E., Rozati, AS., Joshaghani, M., et al."Thermal performance improvement in water nanofluid/GNP–SDBS in novel design of double-layer microchannel heat sink with sinusoidal cavities and rectangular ribs", Journal of Thermal Analysis and Calorimetry, **136**, pp. 1333–1345, (2019).

24. Gholami, M.R., Akbari, A.O., Marzban, A., et al."The effect of rib shape on the behavior of laminar flow of oil/MWCNT nanofluid in a rectangular microchannel", J Therm Anal Calorim, **134**, pp. 1611–1628, (2018).

25. Parsaiemehr, M., Pourfattah, F., Akbari,A.O., et al. "Turbulent flow and heat transfer of Water/Al2O3nanofluid inside a rectangular ribbed channel",Physica E, **96**, pp. 73–84, (2018).

26. Ali, M.M., Rushd, S., Akhter, R., et al."Magneto-hydrodynamic mixed convective heat transfer in a nanofluid filled wavy conduit having rotating cylinders", Scintia Iranica, Transactions on Mechanical Engineering (B), **29(2)**, pp. 486-501, (2022).

27. Farajollahi, A., Mokhtari, A., Rostami, M., et al."Numerical study of using perforated conical turbulators and added nanoparticles to enhance heat transfer performance in heat exchangers", Scintia Iranica, **30(3)**, pp. 1027-1038, (2023).

28. Akbari, A.O.,Toghraie, D., Karimipour, A. "Numerical simulation of heat transfer and turbulent flow of water nano fluids copper oxide in rectangular microchannel with semi attached rib", Adv Mech Eng, **8**, pp. 1–25, (2016).

29. Behnampour, A., Akbari, A.O., Safaei, M.R., et al. "Analysis of heat transfer and nanofluid fluid flow in micro channels with trapezoidal, rectangular and triangular shaped ribs", Phys E, **91**, pp. 15-31, (2017).

30. Mahdy, A."Unsteady mixed convection boundary layer flow and heat transfer of nanofluids due to stretching sheet", Nucl. Eng. Des, **249**, pp. 248-255, (2012).

31. De Brujin, H."The Viscosity of Suspensions of Spherical Particles", Recueil des Travaux Chimiques des Pays-Bas, **61(12)**, pp. 863-874, (1942).

32. Patel, H.E., Sundararajan, T., Pradeep, T., et al."A micro-convection model for thermal conductivity of nanofluids", Pramana J Phys, **65**, pp. 863-869, (2015).

33. Leonard, P.B."A stable and accurate convective modeling procedure based on quadratic upstream interpolation", Comput. Methods Appl. Mech. Eng, **19**, pp. 59-98, (1979).

34. Ahmed, H.F., Kamel, A., Jawad, S.A. "Experimental determination of the optimal location and contraction of sedimentation tank baffles", Water, Air, and Soil Pollution, **92**, pp. 251-271, (1996).

Nomenclature			
Abbreviations	**Descriptions**	**Greek Symbols**	**Description**
c_p	heat capacity $[J\ kg^{-1}K^{-1}]$	μ	dynamic viscosity $(kgm^{-1}s^{-1})$
d_p	nanoparticle size	ρ	density (kg/m^3)
D%	volume fractions of nanoparticle	$\Delta p_1 = \lvert p_{out} - p_{in} \rvert$	absolute pressure drop

$f = \frac{2\Delta p_1 H}{\rho_{nf} L u_{in}^2}$	friction factor	β_{nf}	effective thermal diffusivity
$Nu_{avg} = = \frac{1}{\mathrm{L}}\int \mathrm{Nu(x)\,dx}$	average Nusselt number	$Re = \frac{\rho_{nf} u_{in} H}{\mu_{nf}}$	Reynolds number
$\mathrm{Nu(x)} = \frac{hL}{k_{f_1}}$	local Nusselt number	Pr	Prandtl number
k_{f_1}	thermal conductivity $[Wm^{-1}K^{-1}]$	Pe	Peclet number
u_1, v_1	components of velocity (ms^{-1}) in x and y directions	x, y	Cartesian coordinates (m)
u_0	input velocity	k_b	Bolzmann constant (J/K)
d_{f1}	base fluid molecule diameter	$(\rho c_p)_{nf1}$	nano-fluid heat capacity
d_{np1}	nano-fluid nano particle molecule diameter		
Subscript	**Descriptions**	**Subscript**	**Descriptions**
HT	heat transfer	T_1	temperature (K)
CHT	convective heat transfer	BR	blockage ratio
HE	heat exchange	q	uniform thermal flux
p_1	pressure	FVM	finite volume method
p_{out}	pressure at the outlet	t_0	inlet temperature
p_{in}	pressure at the inlet	H	height of channel (m)
$h(x)$	heat transfer coefficient	N_e	number of elements
H_1	height of obstacle (m)	bf	base-fluid
L	length of channel (m)	t_0	inlet temperature
nf1	nano-fluid	TEF	thermal enhancement factor
m	meter	$\frac{Nu}{Nu_0}$	normalized Nusselt number
ANN	artificial neural network	$np1$	solid nanoparticle
MWCNT	Multi-walled carbon nanotubes		

Table 1: Some excellent works and their obtained results.

Ref.	Authors	Propose geometry	Obtained results
[15]	Wijayantae t al.	double pipe heat exchanger [16] with double-sided delta-wing tape	As compared to a plain tube, T-W inserts with a P/W of 1.18 provide the greatest Nu_{avg}, increasing by about 177%. However, compared to a plain tube, the f is 11.6 times higher, indicating that the friction loss with T-W inserts is more substantial.
[17]	Yaningsih et al.	tube heat exchanger with louvered strip	The findings show that as the slant angle grew increased both HT and the f. With a value of 1.12, the highest slant angle produced the highest thermal performance factor.
[18]	Kristiawan et al.	circular-mini-channel tube	As the concentration of nano-particles grows, the HT performance of the nano-fluid also increases. In the same way, as nano-particle concentration rises, so does the Δp enhancement.

[19]	Kristiawan et al.	square mini-channel	Utilizing simply a nano-fluid with $D\% = 0.01$ can boost the HT in comparison to water running inside the square mini-channel micro-fin.
[20]	Kristiawan et al.	circular tube	They have found that the enhancement of D% causes the increment of CHT coefficient.
[21]	Kristiawan et al.	helical tube	At D%= 0.05, 0.15, and 0.30, Δp decrease inside the microfin tube was 73%, 77%, and 80% higher than that in the smooth tube.
[22]	Kurnia et al.	helical HE	They discovered that, at the expense of a larger Δp, the helical heat exchanger with twisted tape exhibits improved HT performance (higher Nu_{avg}).
[23]	Khodabandeh et al.	double-layer microchannel heat sink	They concluded that the lower wall of the micro-channel's heat resistance decreases and the Nu_{avg} increases with an increase in $D\%$ and Re.
[24, 25]	Gholami et al. and Parsaiemehr et al.	rectangular micro-channel	Their findings show that the presence of obstacles considerably increases the Nu_{avg} and f.
[26]	Ali et al.	wavy conduit with an inclined rotating cylinder	The most notable effects on the HT mechanism were discovered to be caused by the inclined magnetic field, wavy surfaces, and revolving cylinders.
[27]	Farajollahi et al.	heat exchanger with conical turbulator	They demonstrated that, in comparison to the smooth tube, the offered turbulators boost TEF by up to 43%.
[28]	Akbari et al.	rectangular channel with a semi-attached obstacle	They have found that the stronger vortices appear at R/W (length/width)=0.5 as compared to the case of R/W=0.

Table 2: Material characteristics of nano-fluid [24].

Properties	oil, D% = 0 (base fluid)	MWCNT	Nano-fluid, D% = 2	Nano-fluid, D% = 4
$c_p\,(\mathrm{J/kg.K})$	2.032×10^3	17×10^2	20.129×10^2	19.951×10^2
ρ $(\mathrm{kg/m^3})$	2.032×10^3	26×10^2	9.0166×10^2	9.3632×10^2
k $(\mathrm{W/m.K})$	133×10^{-3}	30×10^2	52.55×10^{-2}	79.12×10^{-2}
$\mu(\mathrm{Pa.s})$	289×10^{-4}	---	3.05×10^{-2}	3.21×10^{-2}

Table 3: Maximum velocity at $l_5 = 0.00415\ m, Re = 120$ for $D\% = 0$.

obstacle type	m/s	times of input velocity
Plane	50.492	1.4794
Triangular	50.4877	1.4792
Trapezoidal	50.4849	1.4791
Elliptical	49.9612	1.4638

Table 4: Maximum velocity at $l_6 = 0.00565\ m, Re = 120$ for $D\% = 0$.

obstacle type	m/s	times of input velocity
Plane	50.568	1.4816
Triangular	50.492	1.4794
Trapezoidal	50.4899	1.4793
Elliptical	50.397	1.4698

Table 5: % an increase of f values for different configurations.

obstacle type	f at $D\% = 0$	f at $D\% = 4$	% increase
Plane	9435.711	9767.628	3.517
Triangular	7652.422	8003.129	4.58
Trapezoidal	8051.210	8401.196	4.35
Elliptical	8593.275	8958.313	4.247

Table 6: % an increase of Nu_{avg} values for different obstacle configurations.

obstacle type	Nu_{avg} at $D\% = 0$	Nu_{avg} at $D\% = 4$	% increase
Plane	101.226	103.826	2.567
Triangular	101.210	102.813	1.583
Trapezoidal	101.223	103.413	2.163
Elliptical	100.986	102.166	1.168

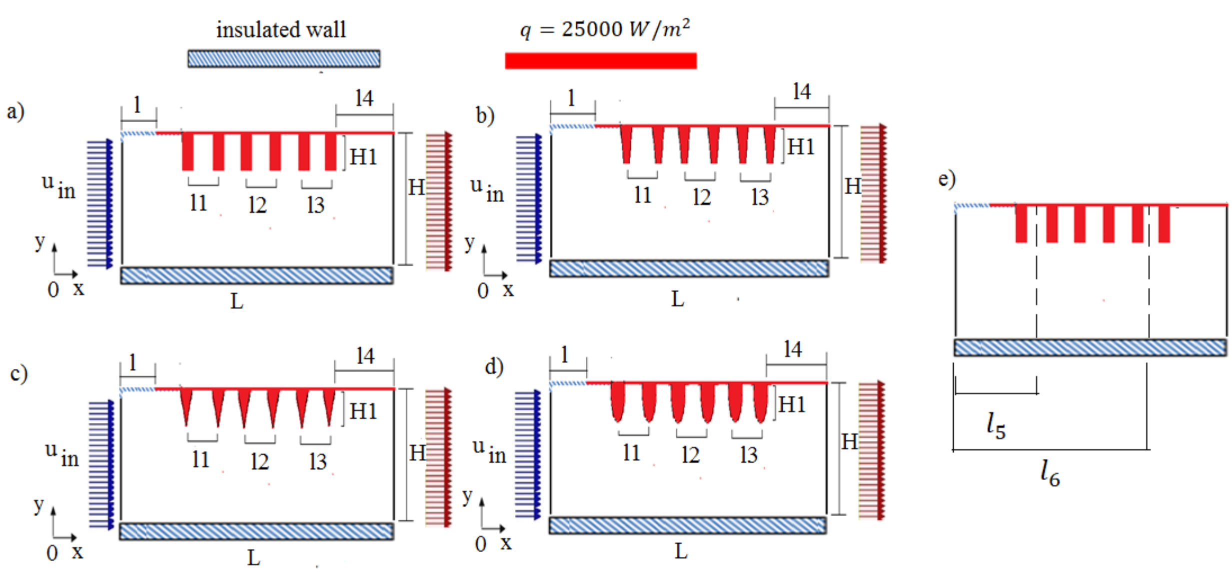

$$H1 = 0.00002\ m, L = 0.0075\ m, l = 0.00375\ m, l1 = l2 = l3 = 0.0025\ \text{m}$$

$$l4 = 0.00225\ \text{m}, H = 0.00005\ m, l_5 = 0.00415\ m, l_6 = 0.00565\ m$$

Figure 1. Rectangular channel embedded with (a) plane, (b) trapezoidal, (c) triangular, (d) elliptical obstacles, and (e) locations of generating plane.

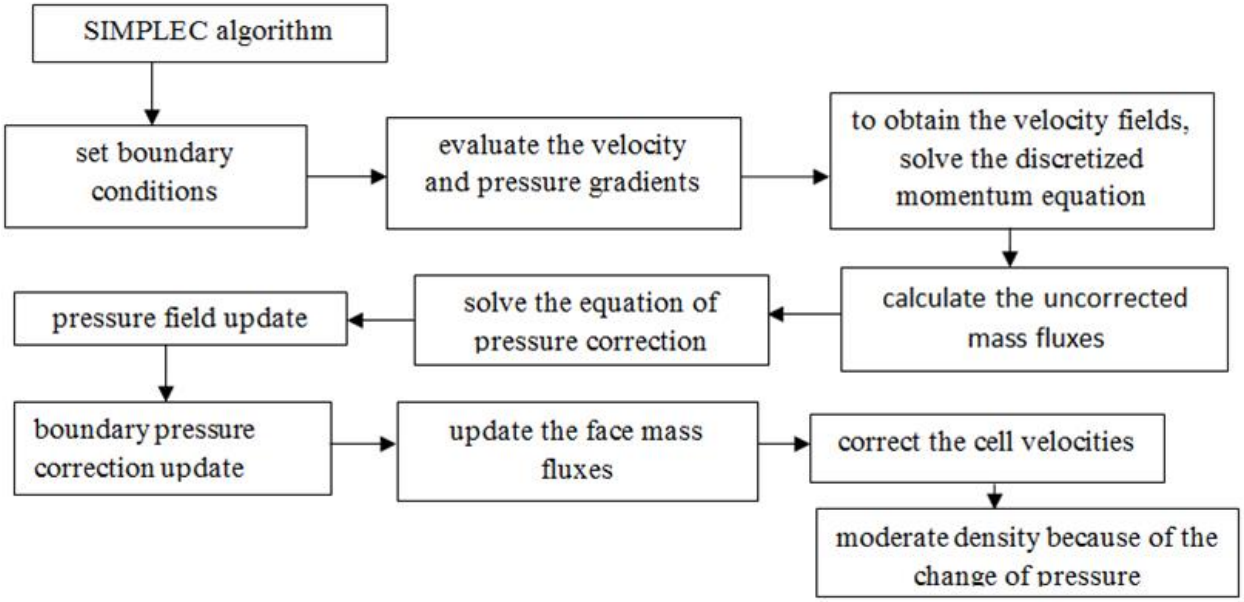

Figure 2. Working procedure of SIMPLEC algorithm.

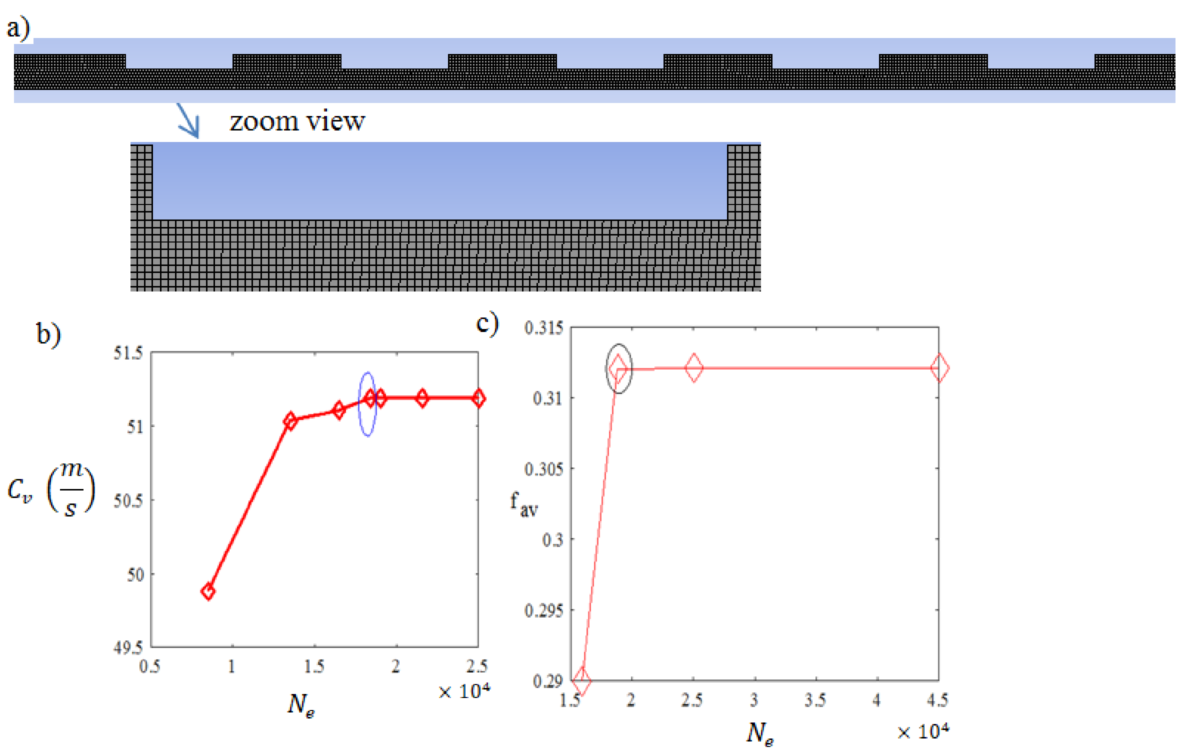

Figure 3. (a) Geometry of mesh configuration, variations of (b) C_v and (c) f_{av} vs. N_e for D% = 0, at $Re = 120$.

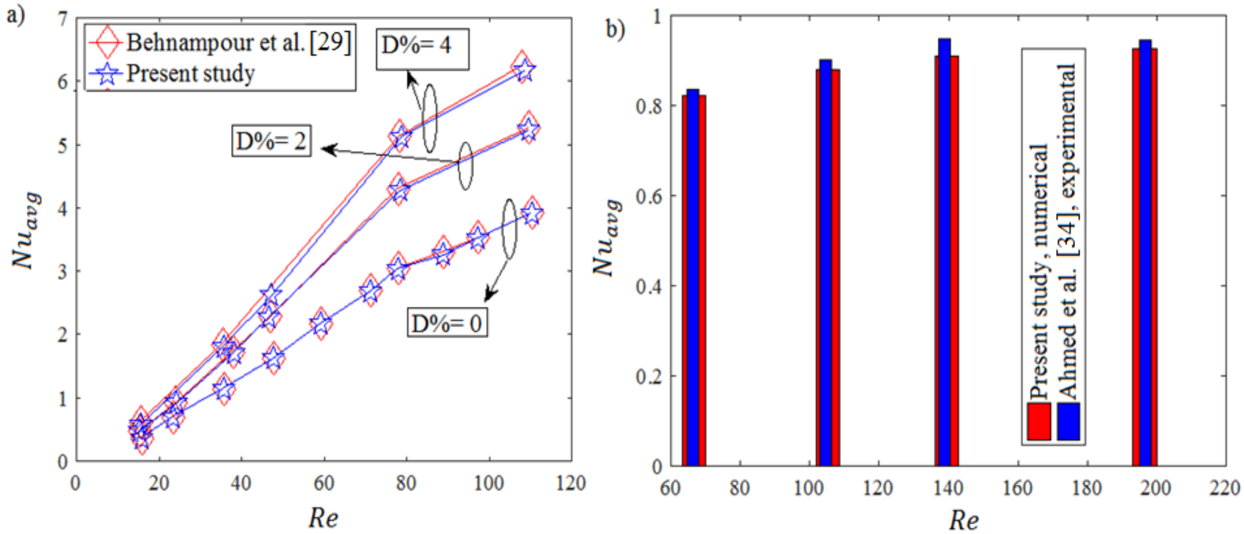

Figure 4.Validation of current study with (a) Behnampour et al. [29], numerical work, (b) Ahmed et al. [34], experimental work by analyzing the profiles of Nu_{avg} vs. Re.

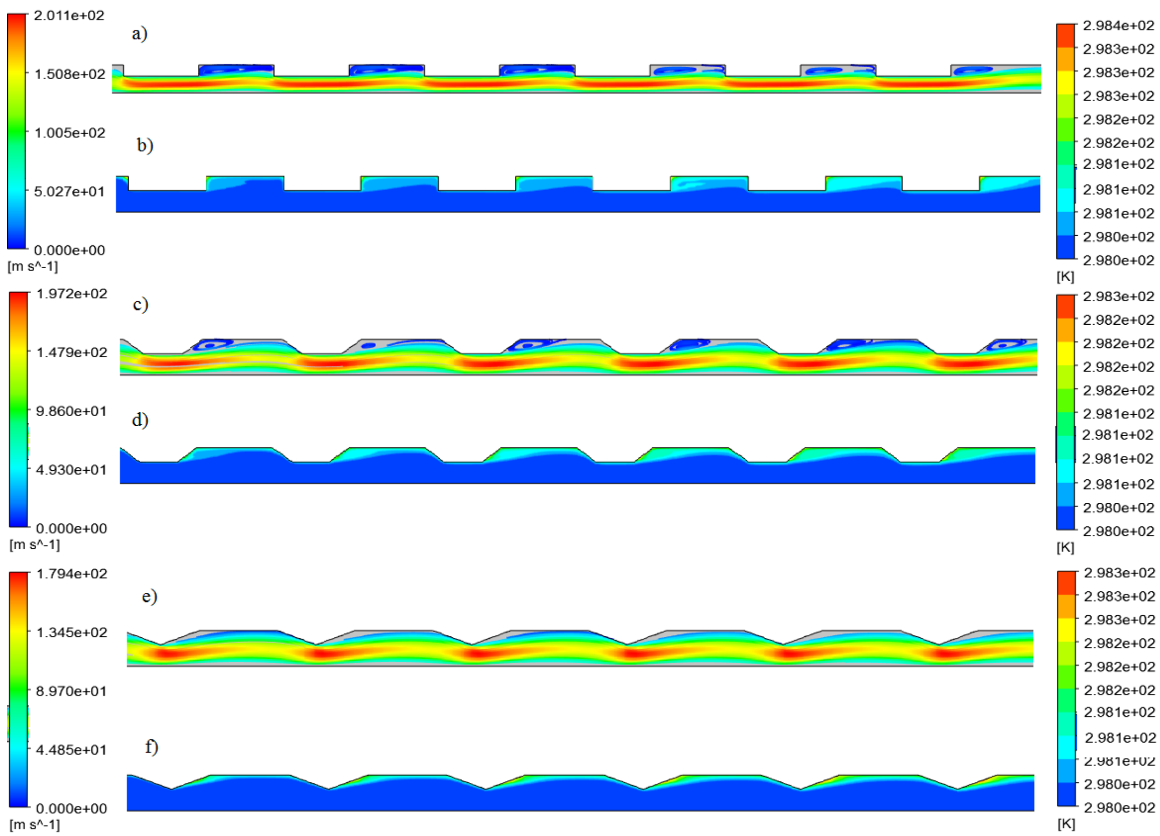

Figure 5. Streamline contour profiles for (a) plane, (c) trapezoidal, (e) triangular obstacle cases, and temperature contour profiles for (b) plane, (d) trapezoidal, (f) triangular obstacle cases at $Re = 120,\ D\% = 4$.

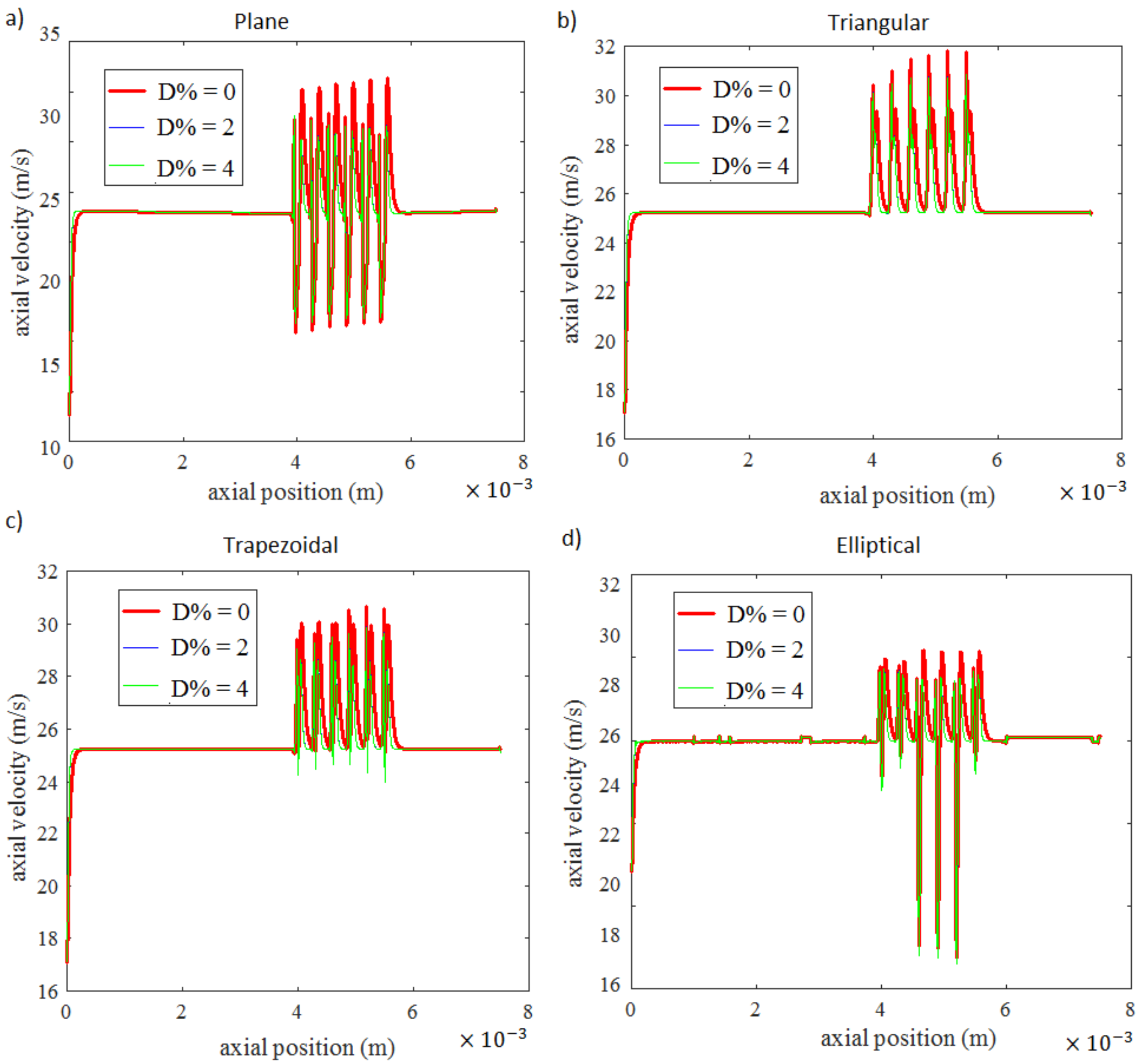

Figure 6. Variations of $D\%$ vs. plots of axial velocity at $Re = 60$ for (a) plane, (b) triangular, (c) trapezoidal, and (d) elliptical obstacle cases along the centerline.

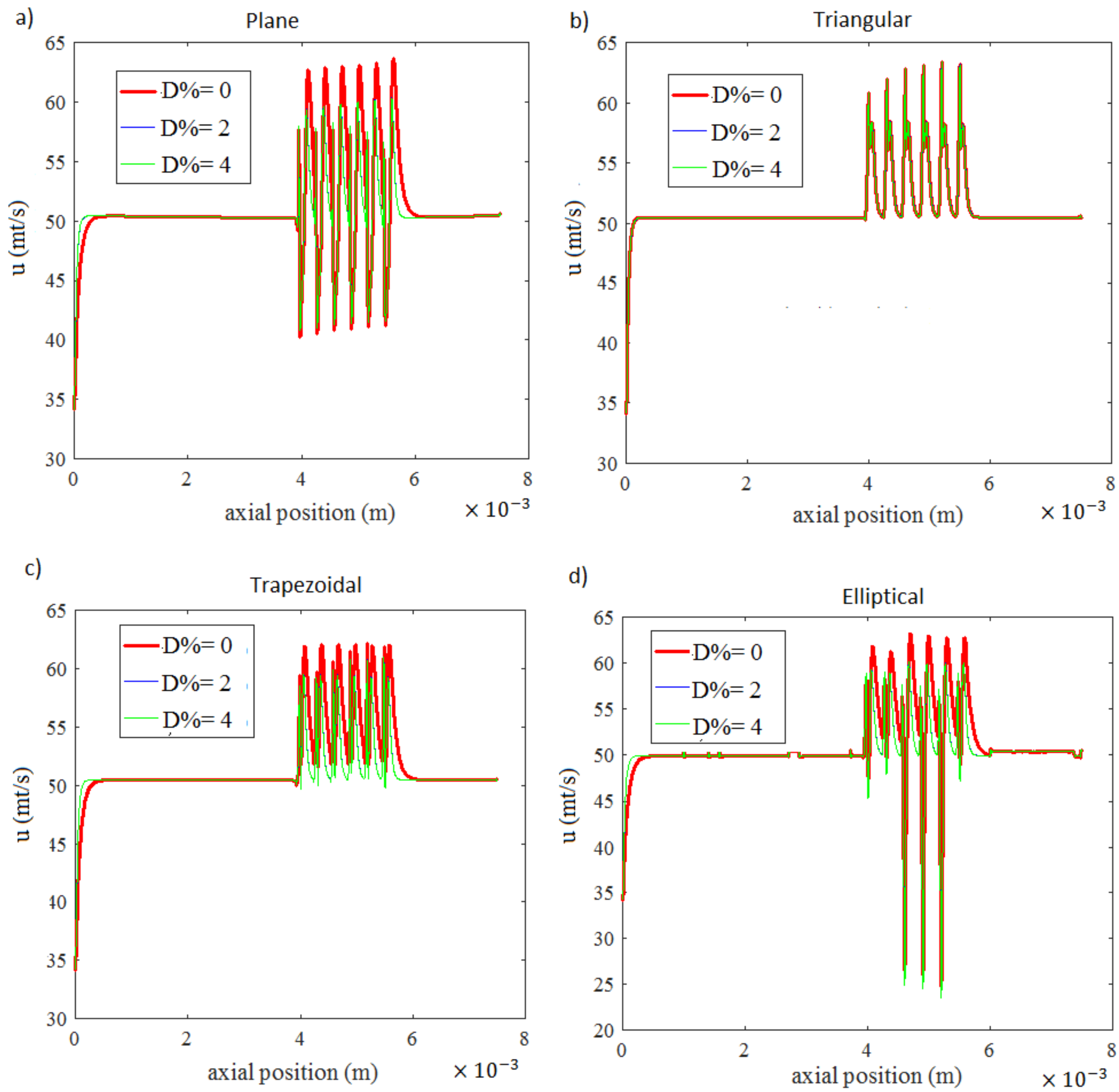

Figure 7. Variations of $D\%$ vs. plots of axial velocity at $Re = 120$ for (a) plane, (b) triangular, (c) trapezoidal, and (d) elliptical obstacle cases along the centerline.

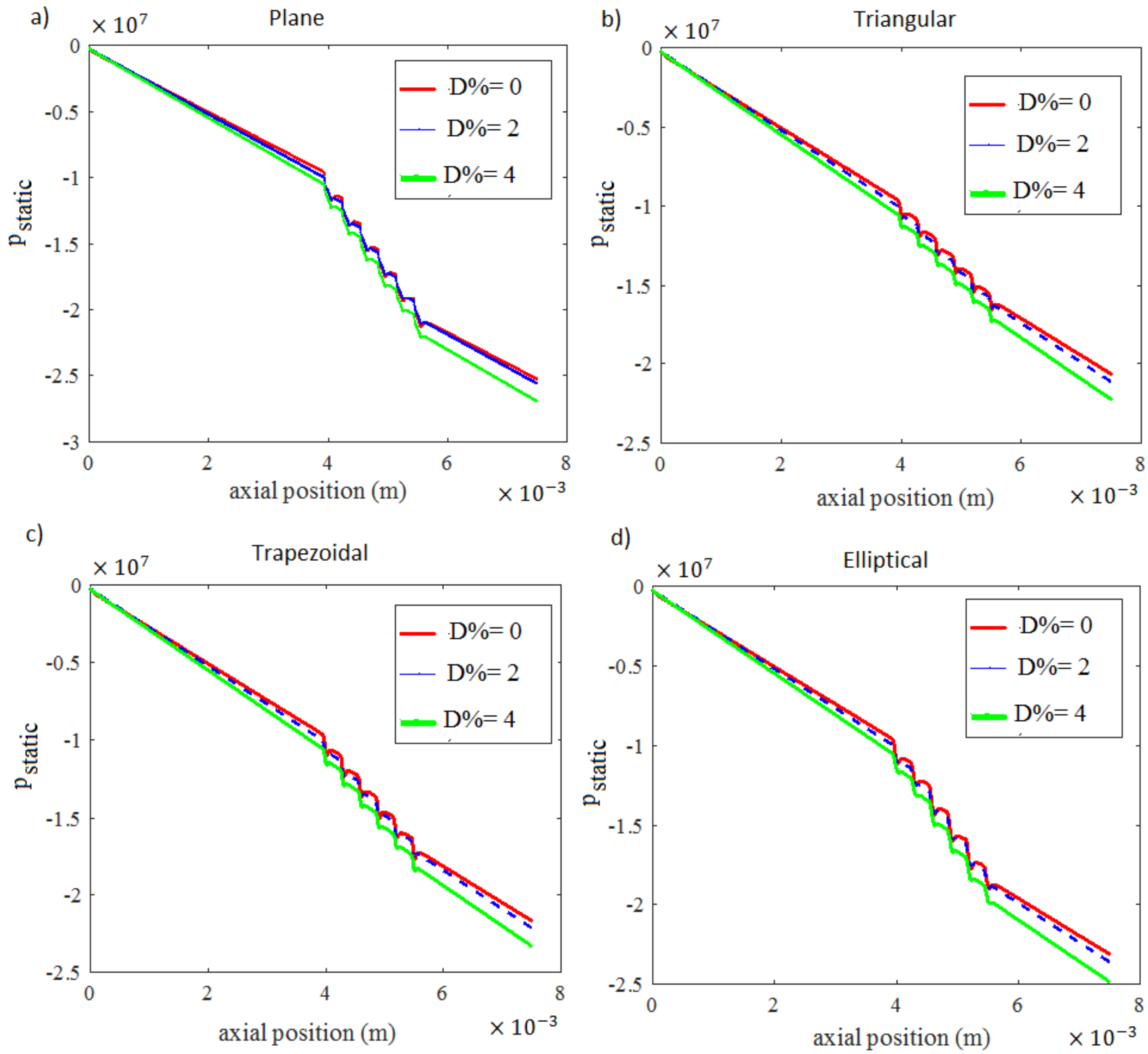

Figure 8. Variations of $D\%$ vs. plots of p_{static} at $Re = 60$ for (a) plane, (b) triangular, (c) trapezoidal, and (d) elliptical obstacle cases along the centerline.

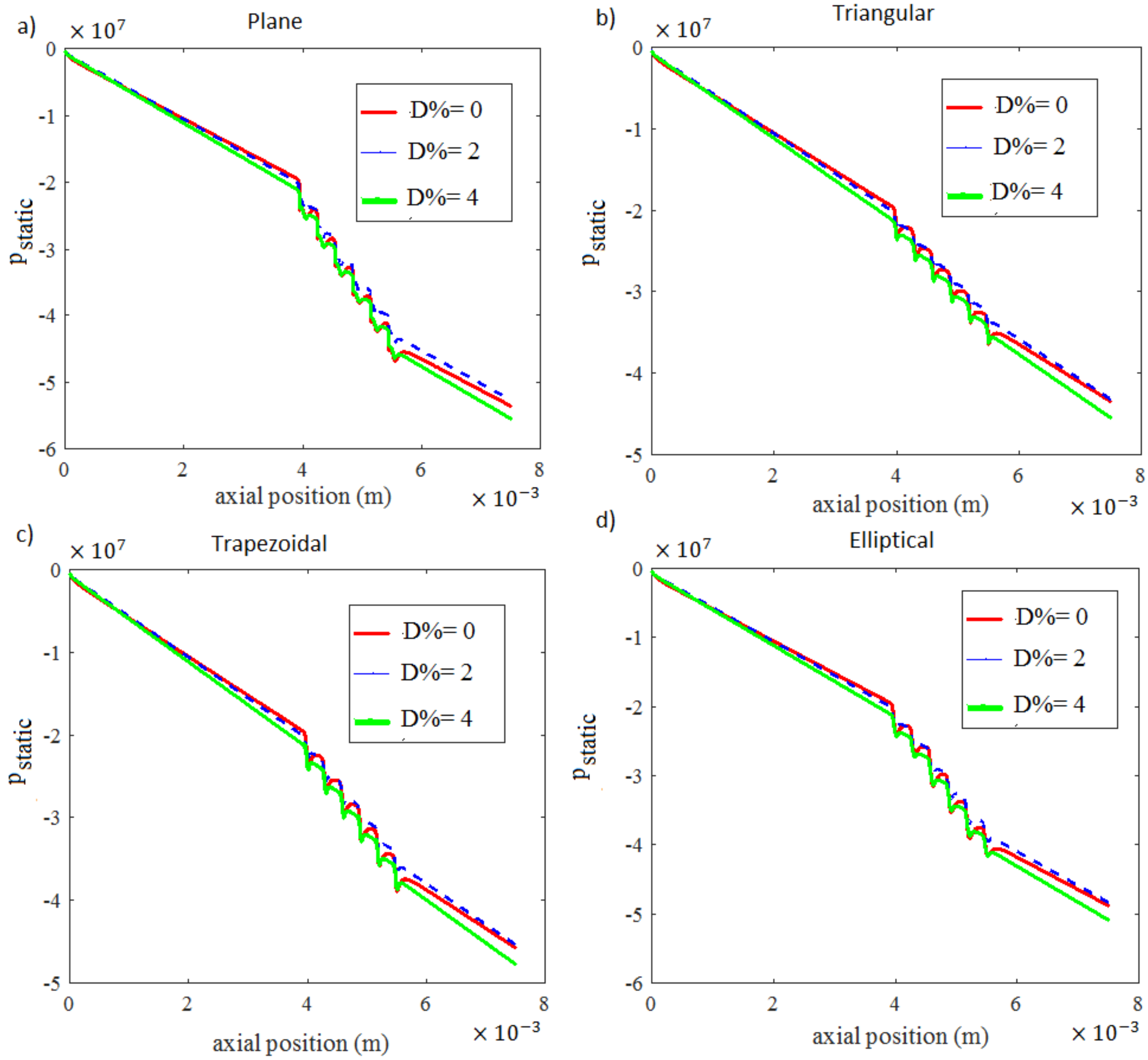

Figure 9.Variations of $D\%$ vs. plots of p_{static} at $Re = 120$ for (a) plane, (b) triangular, (c) trapezoidal, and (d) elliptical obstacle cases along the centerline.

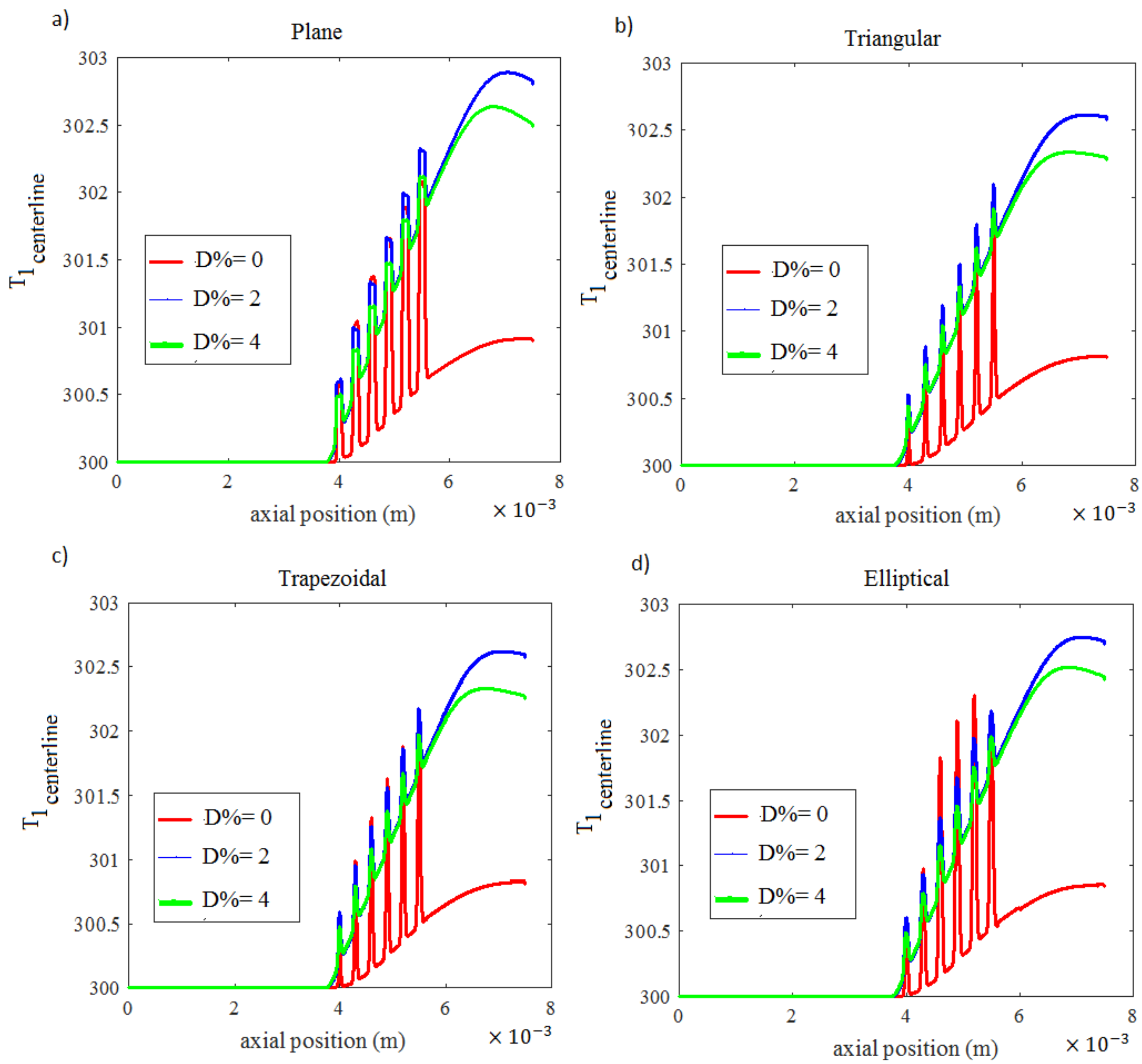

Figure 10.Variations of $D\%$ vs. plots of $T_{1_{centerline}}$ at $Re = 1$ for (a) plane, (b) triangular, (c) trapezoidal, and (d) elliptical obstacle cases along the centerline.

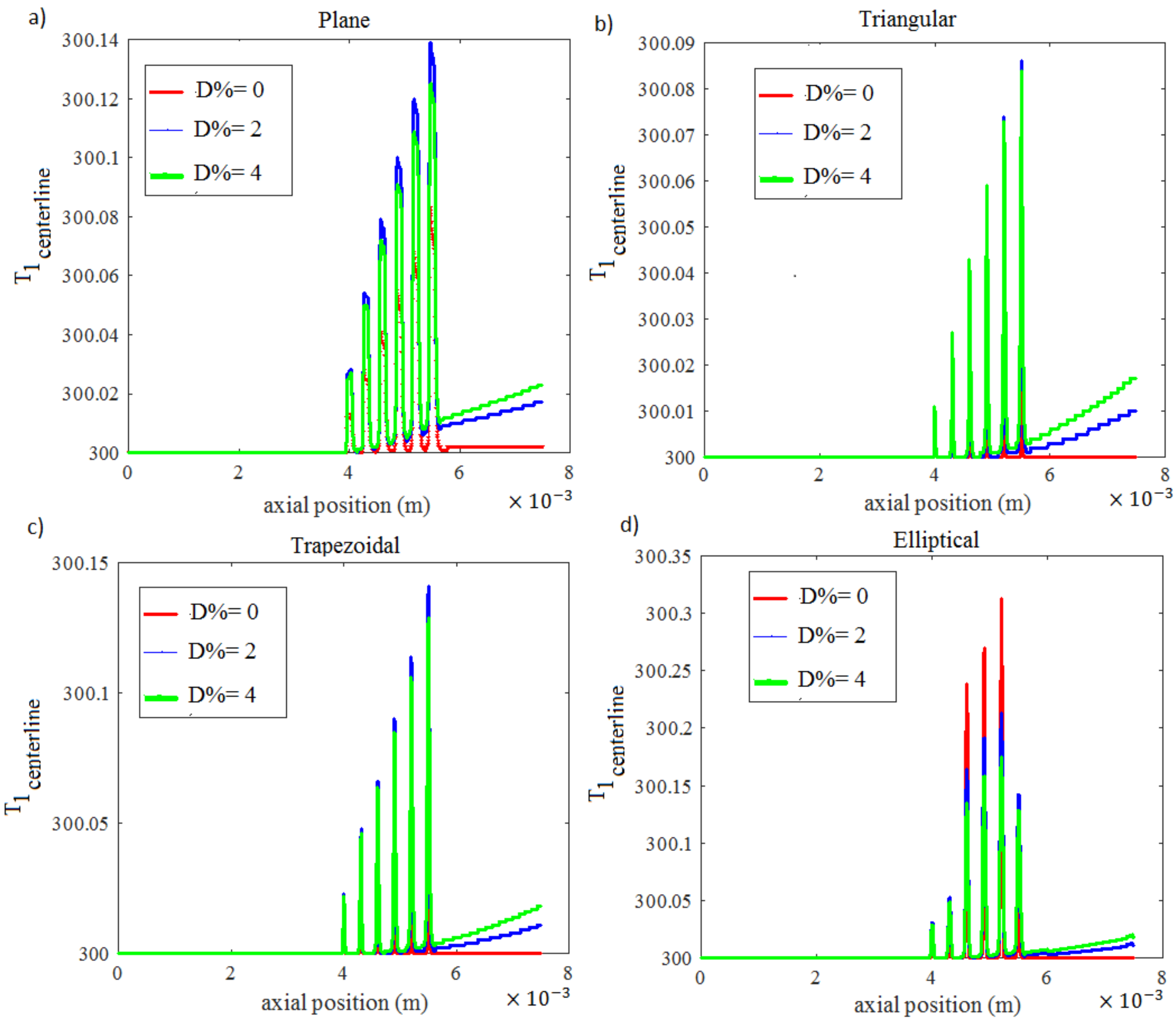

Figure 11.Variations of $D\%$ vs. plots of $T_{1_{centerline}}$ at $Re = 60$ for (a) plane, (b) triangular, (c) trapezoidal, and (d) elliptical obstacle cases along the centerline.

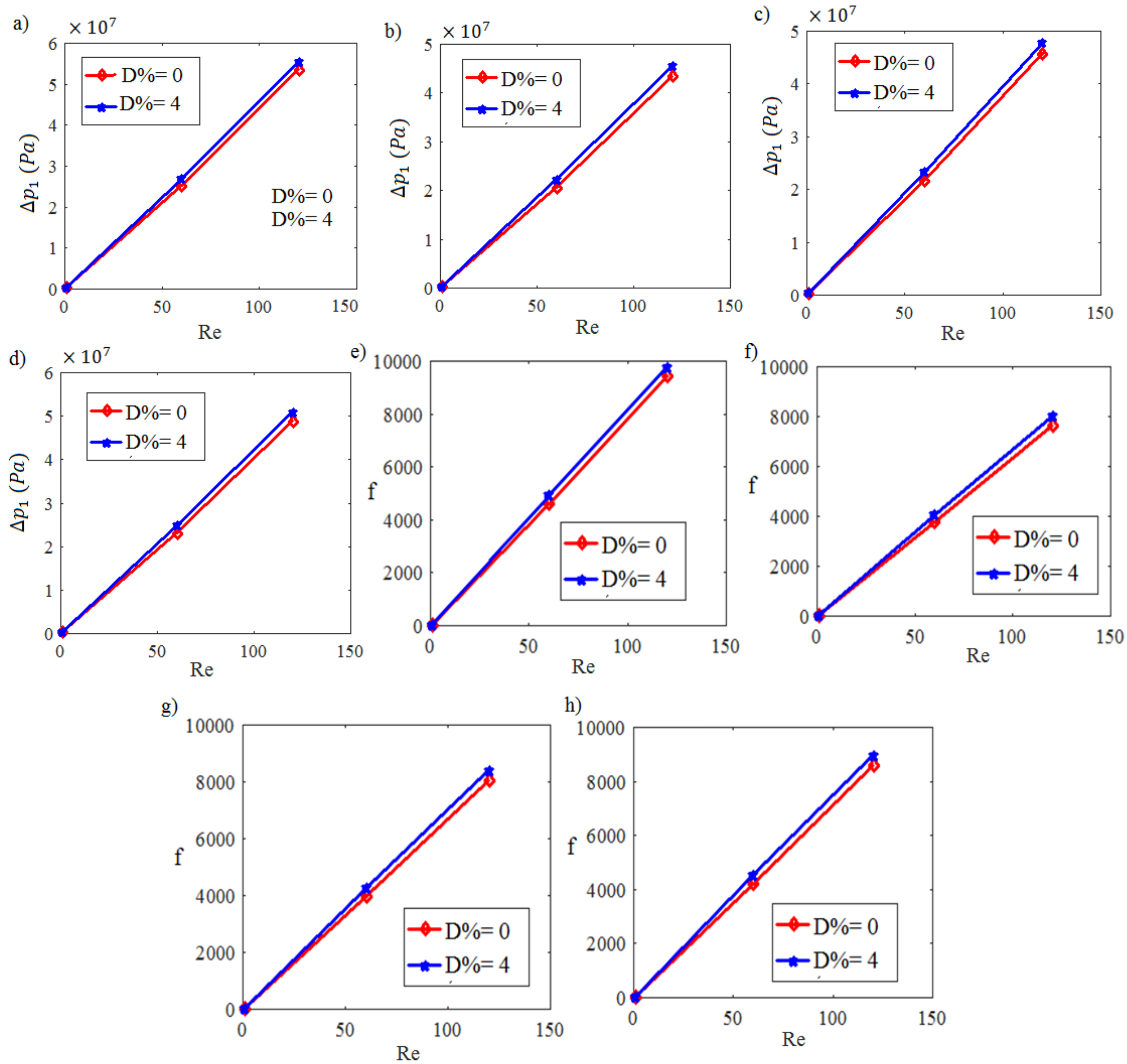

Figure 12. Plots of (a-d) Δp_1, (e-h) f for various $D\%$, Re, and obstacle configurations.

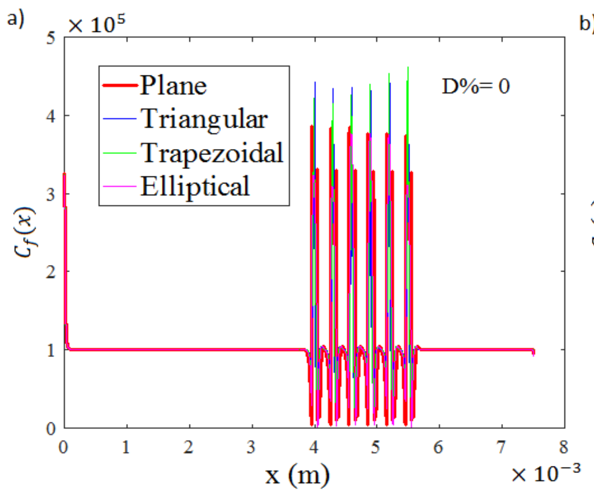

Figure 13. Plots of $C_f(x)$on the heated wall at Re $= (a)120$, (b) 60 for various obstacle configurations.

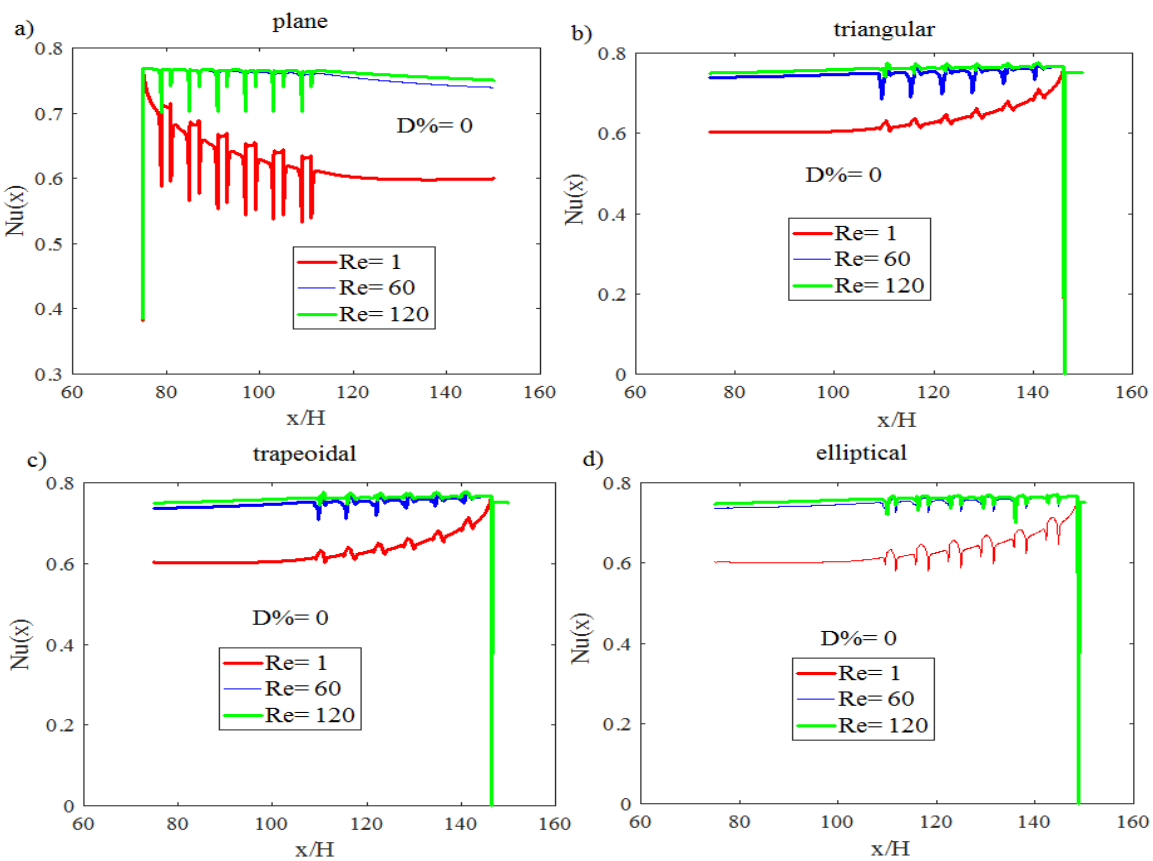

Figure 14. Plots of Nu(x) on the heated wall at (a) $Re = 120$, (b) $Re = 60$ for various obstacle configurations.

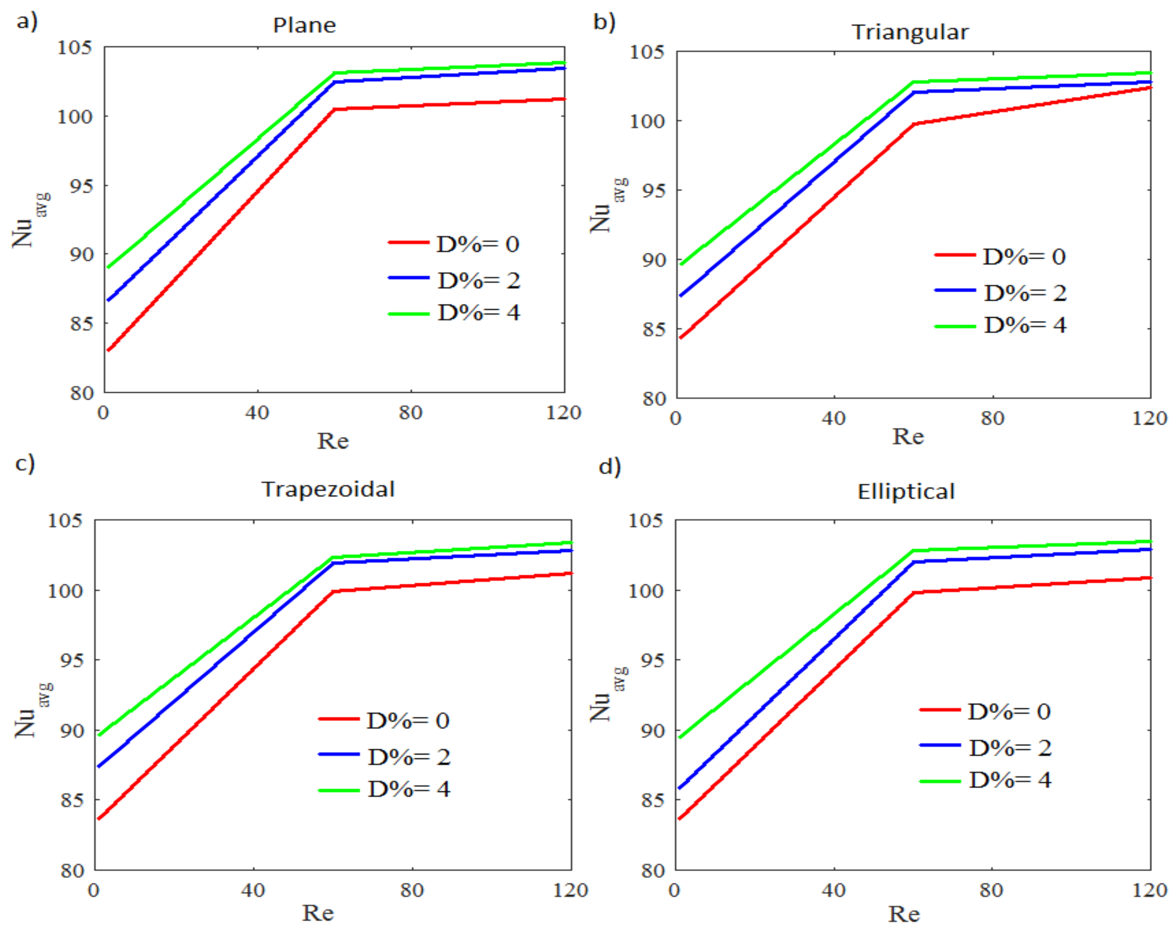

Figure 15. Plots of Nu_{avg} on the heated wall for various Re, and obstacle configurations.

Biographies

Mr. Shahul Hameed was born and raised in Chennai, India. He obtained an MSc degree in Mathematics from The New College (University of Madras) Chennai, India, in 2021. He is a Researcher at Vellore Institute of Technology Chennai, Tamilnadu, India. His research interests are mathematical modeling, Fluid dynamics, properties of nano-fluids, and their heat transfer characteristics.

Dr. Sandip Saha was born and raised in West Bengal, India. He obtained his MSc degree from Indian Institute of Technology Kharagpur, India, in 2013, and Ph.D degrees in Mathematics from National Institute of Technology Silchar, Assam, India. Presently, he is working as an Assistant Professor in the Department of Mathematics, Vellore Institute of Technology Chennai, Tamilnadu, India. Dr. Saha research interest covers the areas of the application of flow separation, particularly in bio-fluid dynamics and analysis of boundary layer flows of Newtonian/non-Newtonian fluids, including entropy generation. Dr. Saha research interest also covers the hybrid nano-fluid flow with entropy generation. He published several papers in national and international journals. He attended several work-shops/seminars/faculty development programs.